Control of chemical reactivity by quantized transition states

ARTICLE *in* THE JOURNAL OF PHYSICAL CHEMISTRY · MARCH 1992

Impact Factor: 2.78 · DOI: 10.1021/j100185a007

Reprinted from The Journal of Physical Chemistry, 1992, 96.

Control of Chemical Reactivity by Quantized Transition States

David C. Chatfield, Ronald S. Friedman, David W. Schwenke, and Donald G. Truhlar*

Department of Chemistry, Supercomputer Institute, and Army High Performance Computing Research Center, University of Minnesota, Minneapolis, Minnesota 55455-0431, and NASA Ames Research Center, Moffett Field, California 94035 *(Received: August 8, 1991; In Final Form: November 1, 1991)*

We review the basic principles of quantized transition state control of microcanonical ensemble rate constants and state-selected rate constants. Selected examples are presented for the H + H_2 and O + H_2 reactions. The following aspects are emphasized: (i) We can calculate accurate quantal microcanonical rate constants up to high energies. (ii) These rate constants show resolvable structure which may be attributed to quantized transition states. (iii) The energy dependence of the microcanonical rate constants can be explained quantitatively using a transition state plus tunneling model based on these quantized transition states. (iv) Fitting the model of quantized transition states plus tunneling to the accurate quantum dynamics yields energies, transmission coefficients, and effective barrier widths for individual energy levels of the transition state. (v) The energy level spectrum can be assigned using the conventional model for a complex with a missing degree of freedom. The spectrum is in good agreement with that predicted by the adiabatic theory of reactions or variational transition state theory. The deviations may provide a quantitative test of approximations typically involved in such calculations, e.g., neglect of anharmonic mode couplings. (vi) The individual transmission coefficients show that the quantitative errors in transition state theory (about 10% at the highest energy considered) result from large breakdowns for a few bend-excited levels rather than from small (say 10%) breakdowns for all transition state levels. (vii) The transition state effective barrier widths can be understood both in terms of the barrier widths of vibrationally adiabatic potential curves and in terms of resonance theory. (viii) Transition state resonance theory also allows predictions of transition state lifetimes on the basis of fits to the energy derivative of the microcanonical rate constant. (ix) We can calculate half-collision transition probabilities for specific reactant states to proceed to particular states of the activated complex and for particular states of the activated complex to proceed to specific states of the products; this allows for a very detailed picture of how state-to-state reactions occur. (x) The analysis of state-selected reactivity in terms of passage through particular transition states explains trends in the dependence of rate constants on initial vibrational and rotational quantum numbers.

Introduction

In 1935 Eyring[1] presented the transition state theory rate expression that is still widely used today. This formula makes the chemical reaction rate constant for a canonical ensemble proportional to a "transition state partition function" which is a sum over states of an activated complex with quantized energy levels. Similarly, the microcanonical ensemble version of transition state theory—widely used, e.g., in the RRKM theory[2] of unimolecular rates—yields the expression

$$k^{\ddagger}(E) = N^{\ddagger}(E)/h\rho^{R}(E) \qquad (1)$$

for the rate constant $k^{\ddagger}(E)$ at a given energy E, where $N^{\ddagger}(E)$ is the number of energy states of the transition state with energies less than or equal to E, h is Planck's constant, and $\rho^{R}(E)$ is the density of states of the reactant. Transition state theory in both the canonical and microcanonical versions has been enormously successful,[3] especially when the transition state is determined variationally,[4] but until very recently there has been no direct evidence for a quantized spectrum of the transition state. We have,

* To whom correspondence should be addressed at the University of Minnesota.

(1) Eyring, H. *J. Chem. Phys.* **1935**, *3*, 107. See also: Wigner, E. *Z. Phys. Chem., Abt. B* **1932**, *15*, 203. Evans, M. G.; Polanyi, M. *Trans. Faraday Soc.* **1935**, *31*, 875.

(2) (a) Marcus, R. A.; Rice, O. K. *J. Phys. Colloid Chem.* **1951**, *55*, 894. Marcus, R. A. *J. Chem. Phys.* **1952**, *20*, 359. See also: Magee, J. L. *Proc. Natl. Acad. Sci. U.S.A.* **1952**, *38*, 764. Quack, M.; Troe, J. *Spec. Period. Rep.: Gas Kinet. Energy Transfer* **1977**, *2*, 175. (b) For bimolecular reactions see: Marcus, R. A. *J. Chem. Phys.* **1966**, *45*, 2138. Note that in eq 1 $\rho^{R}(E)$ is the density of states per unit energy for unimolecular reactions and the density of states per unit energy per unit volume for bimolecular reactions.

(3) Truhlar, D. G.; Hase, W. L.; Hynes, J. T. *J. Phys. Chem.* **1983**, *87*, 2664, 5523 (E).

(4) Wigner, E. *J. Chem. Phys.* **1937**, *5*, 720. Horiuti, J. *Bull. Chem. Soc. Jpn.* **1938**, *13*, 210. Truhlar, D. G.; Garrett, B. C. *Annu. Rev. Phys. Chem.* **1984**, *35*, 159. Tucker, S. C.; Truhlar, D. G. In *New Theoretical Concepts for Understanding Organic Reactions*; Bertrán, J., Csizmadia, I. G., Eds.; Kluwer: Dordrecht, 1986; p 47.

0022-3654/92/2096-2414$03.00/0

however, recently reported[5,6] the observation of such a spectrum in accurate quantum dynamics calculations for the reaction H + H_2 → H_2 + H, and we have assigned 39 levels. Earlier, Bowman showed that our accurate quantum dynamics calculations[7] on O + H_2 → OH + H gave evidence for one or two bend-excited transition state energy levels,[8] and recently in more extensive calculations we have found and assigned about 20 levels in the quantized transition state spectrum for that reaction.[9] In addition, Darakjian et al.[10] have recently found evidence for quantized transition state energy levels in the reaction He + H_2^+ → HeH^+ + H, and new analyses[11] of the calculations of Schatz[12-14] for the Cl + HCl, I + HI, and I + DI reactions have shown that the broad structure of the cumulative reaction probabilities may be understood in terms of quantized transition states for those cases, too; we have assigned seven of the transition state energy levels for Cl + HCl, five for I + HI, and seven for I + DI. The transition state spectrum is not necessarily easy to "see" in the reaction probabilities themselves, or even in the microcanonical ensemble rate constants, because the transition state energy levels do not couple to all reactant or product states equally strongly, and they may be closely spaced compared to the level widths. We have, however, developed methods for seeing and analyzing the transition state spectrum in simple reactions. The present article discusses these methods and selected results.

Quantized transition states can be thought of as dynamical bottlenecks which gate the flow of reactive flux from reactants to products. Previously, the success of generalized transition state theory calculations in reproducing accurate quantum dynamical rate constants had given us considerable confidence that quantized dynamical bottlenecks determine the overall threshold energy of chemical reactivity.[15-20] In our recent work, we have shown[5] that dynamical bottlenecks not only control the chemical reactivity at the threshold to reaction but also in fact globally control chemical reactivity over the entire range of energies relevant to thermal rate constants, even for very high temperatures for the H + H_2 reaction.

We have been able to determine transmission coefficients for individual levels of the transition state[5,6,9,11] and also to determine[6,9] which individual states of the reactants contribute to the reactive flux passing through specific levels of the transition state. This latter kind of analysis leads to a new level of understanding of state-selected reactivity. In this paper we provide an introduction to the key ideas and illustrate their use.

Theory

An exact quantum mechanical expression for the microcanonical rate constant in terms of state-selected reaction probabilities $P_n(E)$ is given by[2b,5]

$$k(E) = [h\rho^R(E)]^{-1}\sum_n P_n(E) \tag{2}$$

where n is an index of the quantum state of the reactants. In terms of state-to-state reaction probabilities, $P_{nn'}(E)$, where n' is an index of the quantum state of the products, the state-selected reaction probabilities are defined by

$$P_n(E) = \sum_{n'} P_{nn'}(E) \tag{3}$$

The final sum in eq 2 contains all the dynamics in both the microcanonical and canonical rate constants, and it plays an important role in the derivation of transition state theory for both canonical[18,21-29] and microcanonical[2b,5,18] ensembles; it is called[25] the cumulative reaction probability, defined by

$$N(E) = \sum_n \sum_{n'} P_{nn'}(E) \tag{4}$$

Transition state theory provides a useful framework for understanding the energy dependence of the cumulative reaction probability and hence the accurate rate constant. For instance, by comparing (1) and (2) we see that transition state theory predicts that $h\rho^R(E)k(E)$ will increase in steps of unity at the transition state energy levels. However, the version of transition state theory that leads to (1) neglects the quantum mechanical probability of tunneling through a reaction barrier and assumes that the transition state is a perfect dynamical bottleneck, i.e., that systems crossing the transition state arrive directly from reactants and proceed directly to products without recrossing.[4] The simplest way to correct for the breakdown of these assumptions is to replace (1) by[18,30]

$$k^{\ddagger}(E) = \frac{\sum_\tau \kappa_\tau P_\tau^{\ddagger}(E - E_\tau)}{h\rho^R(E)} \tag{5}$$

where the numerator still contains a sum over energy levels E_τ but—instead of increasing by one when a new transition state energy level is surmounted—has an increase governed by the product of a transmission coefficient κ_τ times a quantal or semiclassical transmission probability $P_\tau^{\ddagger}(E - E_\tau)$. If we associate an effective energy barrier V_τ with each level τ and for simplicity assume that this barrier is parabolic as a function of a reaction coordinate s, i.e.

$$V_\tau = E_\tau + \tfrac{1}{2}k_\tau s^2 \tag{6}$$

with k_τ a negative force constant, then this yields[31,32]

$$P_\tau^{\ddagger}(E - E_\tau) = \frac{1}{1 + \exp[(E_\tau - E)/W_\tau]} \tag{7}$$

(5) Chatfield, D. C.; Friedman, R. S.; Truhlar, D. G.; Garrett, B. C.; Schwenke, D. W. *J. Am. Chem. Soc.* **1991**, *113*, 486.
(6) Chatfield, D. C.; Friedman, R. S.; Truhlar, D. G.; Schwenke, D. W. *Faraday Discuss. Chem. Soc.* **1991**, *91*, 289.
(7) Haug, K.; Schwenke, D. W.; Truhlar, D. G.; Zhang, Y.; Zhang, J. Z. H.; Kouri, D. J. *J. Chem. Phys.* **1987**, *87*, 1892 and unpublished. Zhang, J. Z. H.; Zhang, Y.; Kouri, D. J.; Garrett, B. C.; Haug, K.; Schwenke, D. W.; Truhlar, D. G. *Faraday Discuss. Chem. Soc.* **1987**, *84*, 371.
(8) Bowman, J. M. *Chem. Phys. Lett.* **1987**, *141*, 545. See also: Bowman, J. M. *J. Phys. Chem.* **1991**, *95*, 4960.
(9) Chatfield, D. C.; Friedman, R. S.; Lynch, G. C.; Truhlar, D. G.; Schwenke, D. W. Manuscript in preparation.
(10) Darakjian, Z.; Hayes, E. F.; Parker, G. A.; Butcher, E. A.; Kress, J. D. *J. Chem. Phys.* **1991**, *95*, 2516.
(11) Chatfield, D. C.; Friedman, R. S.; Lynch, G. C.; Truhlar, D. G. *Faraday Discuss. Chem. Soc.* **1991**, *91*, 398; *J. Phys. Chem.* **1992**, *96*, 57.
(12) Schatz, G. C. *J. Chem. Phys.* **1989**, *90*, 3582.
(13) Schatz, G. C. *J. Chem. Phys.* **1989**, *90*, 4847.
(14) Schatz, G. C. *J. Chem. Soc., Faraday Trans.* **1990**, *86*, 1729.
(15) Truhlar, D. G.; Kuppermann, A. *J. Chem. Phys.* **1972**, *56*, 2232.
(16) (a) Bowman, J. M.; Kuppermann, A.; Adams, J. T.; Truhlar, D. G. *Chem. Phys. Lett.* **1973**, *20*, 229. (b) Duff, J. W.; Truhlar, D. G. *Chem. Phys. Lett.* **1973**, *23*, 327.
(17) Schatz, G. C.; Kuppermann, A. *J. Chem. Phys.* **1976**, *65*, 4668.
(18) Garrett, B. C.; Truhlar, D. G. *J. Phys. Chem.* **1979**, *83*, 1079.
(19) Truhlar, D. G.; Garrett, B. C. *Acc. Chem. Res.* **1980**, *13*, 440.
(20) (a) Truhlar, D. G.; Isaacson, A. D.; Skodje, R. T.; Garrett, B. C. *J. Phys. Chem.* **1982**, *86*, 2252. (b) Garrett, B. C.; Truhlar, D. G.; Schatz, G. C. *J. Am. Chem. Soc.* **1986**, *108*, 2876. (c) Truhlar, D. G.; Garrett, B. C. *J. Chim. Phys.* **1987**, *84*, 365. (d) Lynch, G. C.; Truhlar, D. G.; Garrett, B. C. *J. Chem. Phys.* **1989**, *90*, 3102.
(21) Eyring, H.; Walter, J.; Kimball, G. E. *Quantum Chemistry*; John Wiley & Sons: New York, 1944; p 306.
(22) Marcus, R. A. *J. Chem. Phys.* **1967**, *46*, 959.
(23) Truhlar, D. G. *J. Chem. Phys.* **1970**, *53*, 2041.
(24) Miller, W. H. *J. Chem. Phys.* **1974**, *61*, 1823.
(25) Miller, W. H. *J. Chem. Phys.* **1975**, *62*, 1899.
(26) Kuppermann, A. *J. Phys. Chem.* **1979**, *83*, 171.
(27) Christov, S. G. *Collision Theory and Statistical Theory of Chemical Reactions*; Springer-Verlag: Berlin, 1980.
(28) Truhlar, D. G.; Isaacson, A. D.; Garrett, B. C. In *Theory of Chemical Reaction Dynamics*; Baer, M., Ed.; CRC Press: Boca Raton, FL, 1985; p 65.
(29) (a) Bowman, J. M.; Wagner, A. F. In *The Theory of Chemical Reaction Dynamics*; Clary, D. C., Ed.; Reidel: Dordrecht, 1986; p 47. (b) Sun, Q.; Bowman, J. M.; Schatz, G. C.; Sharp, J. R.; Connor, J. N. L. *J. Chem. Phys.* **1990**, *92*, 1677.
(30) Marcus, R. A. *J. Chem. Phys.* **1965**, *43*, 1598. Marcus, R. A. In *Investigation of Rates and Mechanisms of Reactions*, 3rd ed.; Lewis, E. S., Ed.; Wiley-Interscience: New York, 1974; Part I, p 13.
(31) Kemble, E. C. *The Fundamental Principles of Quantum Mechanics*; Dover: New York, 1958.
(32) In principle, eq 6 should be truncated so $V_\tau \geq 0$ and $P_\tau^{\ddagger} = 0$ for $E \leq 0$. In practice, for the cases considered here, $E_\tau \gg W_\tau$, and this holds to an excellent approximation. In the same spirit the normalization integral below eq 11 holds only if the lower limit is extended to $-\infty$.

where the width parameter is given by

$$W_\tau = \hbar|\omega_\tau|/2\pi \tag{8}$$

$$\omega_\tau = (k_\tau/\mu)^{1/2} \tag{9}$$

and μ is the reduced mass. The transmission probability $P_\tau^\dagger(E - E_\tau)$, which rises smoothly from 0 to 1, accounts for tunneling at energies below the barrier height and nonclassical reflection at higher energies. The deviation of the transmission coefficient κ_τ from unity accounts for the breakdown of transition state theory due to systems that recross the variational transition state and to other multidimensional effects.[4]

Taking the derivative of $h\rho^R(E)k^\dagger(E)$ yields, from eqs 5 and 7, the density of states

$$\rho^\dagger(E) \equiv \sum_\tau \kappa_\tau \rho_\tau(E) \tag{10}$$

where

$$\rho_\tau(E) = \frac{\exp[(E_\tau - E)/W_\tau]}{W_\tau\{1 + \exp[(E_\tau - E)/W_\tau]\}^2} \tag{11}$$

The function $\rho_\tau(E)$ is a symmetric bell-shaped curve centered at E_τ, and the value of the integral $\int_0^\infty \rho_\tau(E)\,dE$ is one.[32]

The quantum mechanical analogue of the transition state theory $\rho^\dagger(E)$ is the density of reactive states, defined as

$$\rho(E) \equiv \frac{d}{dE}\left(\sum_n \sum_{n'} P_{nn'}(E)\right) \tag{12}$$

Transition state theory with the semiclassical refinements of the previous paragraph predicts that $h\rho^R(E)k(E)$ [or, equivalently, $N(E)$, but we emphasize the microcanonical ensemble rate constant to make the connection to experiment more clear] will increase in a smoothed-out step of height κ_τ at each transition state energy level and that the density of reactive states $\rho(E)$ will be a sum of bell-shaped curves, each with area κ_τ, centered at the transition state energy levels. We have found that it is the quantity $\rho(E)$ that most clearly reveals the quantized transition state spectrum for the reactions we have studied. We have found that the accurate quantum mechanical $\rho(E)$ for these reactions exhibits the type of behavior predicted by transition state theory.

Since total angular momentum (J) is conserved during a collision, the reaction dynamics can be studied for each value of J independently. This allows the calculation of total-angular-momentum-specific contributions to the rate constant, $k^J(E)$, and to the density of reactive states, $\rho^J(E)$. The overall rate constant $k(E)$ is a sum of the individual $k^J(E)$, each weighted by $(2J + 1)$, and so the influence of quantized transition states on $k(E)$ can be determined by studying the individual $k^J(E)$.

Converged quantum dynamics calculations were carried out for realistic potential energy surfaces using the generalized Newton variational principle.[33] In this method the Schrödinger equation and its boundary conditions are first expressed as an integral equation, which is then reformulated in terms of the reactive amplitude density. The reactive amplitude density is expanded in a square-integrable basis set, and a variational principle is used to solve for all state-to-state reaction probabilities with a given E and J, taking full account of parity and arrangement symmetry to simplify the calculations. The basis and numerical parameters were chosen to converge the sum of the reaction probabilities over all initial and final states to calculate microcanonical ensemble rate constants. Numerical "noise" must be small so that numerical differentiation with respect to energy yields smooth densities. The calculations[5,6,9] discussed in this account were carried out using an accurate potential energy function[34] for the H + H_2 reaction and a realistic potential energy function[35] for the O + H_2 reaction.

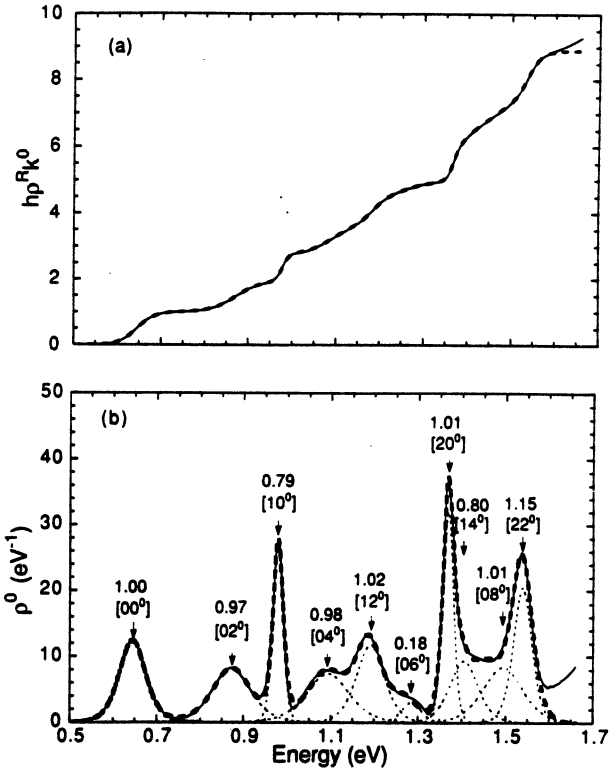

Figure 1. H + H_2, $J = 0$. (a) Cumulative reaction probability. The solid curve is a spline fit to accurate quantal results, and the dashed curve is obtained by integrating the synthetic density curve shown in Figure 1b. (b) Density of reactive states. The solid curve is obtained by differentiating the solid curve in Figure 1a, and the heavy dashed curve is the fit of (10) and (11). The light dashed lines are the individual terms in the sum in (10). The arrows are positioned at the E_τ values from the fit, and the numbers indicate the value of κ_τ for each feature.

Examples

The product $h\rho^R(E)k^0(E)$ for the reaction of H with H_2 is shown as a function of energy as the solid line in Figure 1a. Close inspection reveals steplike features suggestive of the behavior predicted by transition state theory. The derivative of $h\rho^R(E)k^0(E)$ is the density of reactive states $\rho^0(E)$, shown as the solid line in Figure 1b. Taking the derivative converts the steplike features into peaks. At 1.6 eV, the upper end of the energy range studied, $h\rho^R(E)k^0(E)$ reaches a value of 8.9. Thus transition state theory would lead us to believe there should be nine energy levels of a quantized transition state below 1.6 eV, if all κ_τ are unity, or more if transition state theory overestimates the rate. (Transition state theory would always overestimate the rate if atoms obeyed classical mechanics.[4] This provides a guide to the quantum mechanical world where there is no strict bound.) Seven peaks and one shoulder are readily apparent in Figure 1b, and we identify these with the energy levels of a quantized transition state. The more detailed analysis discussed in the next paragraph identifies two unresolved states, for a total of 10.

We "resolved" the spectrum $\rho^0(E)$ by modeling the contribution due to each energy level of the transition state according to semiclassical transmission through effective parabolic energy barriers using eqs 5–11. The accurate quantum mechanical density of reactive states $\rho^0(E)$ is fit with a sum of terms $\kappa_\tau\rho_\tau(E)$, each corresponding to an energy level of the transition state, according to (10). The individual $\rho_\tau(E)$ are expressed according to (11), and the quantities κ_τ, E_τ, and W_τ are treated as adjustable parameters. A fit with 10 terms included in the sum very accurately reproduces the quantal $\rho^0(E)$. The individual terms $\kappa_\tau\rho_\tau(E)$ are

(33) Schwenke, D. W.; Haug, K.; Truhlar, D. G.; Sun, Y.; Zhang, J. Z. H.; Kouri, D. J. *J. Phys. Chem.* **1987**, *91*, 6080. Schwenke, D. W.; Haug, K.; Zhao, M.; Truhlar, D. G.; Sun, Y.; Zhang, J. Z. H.; Kouri, D. J. *J. Phys. Chem.* **1988**, *92*, 3202. Schwenke, D. W.; Mladenovic, M.; Zhao, M.; Truhlar, D. G.; Sun, Y.; Kouri, D. J. In *Supercomputer Algorithms for Reactivity, Dynamics and Kinetics of Small Molecules*; Laganà, A., Ed.; Kluwer: Dordrecht, 1989; p 131. Sun, Y.; Yu, C.-h.; Kouri, D. J.; Schwenke, D. W.; Halvick, P.; Mladenovic, M.; Truhlar, D. G. *J. Chem. Phys.* **1989**, *91*, 1643.

(34) Varandas, A. J. C.; Brown, F. B.; Mead, C. A.; Truhlar, D. G.; Blais, N. C. *J. Chem. Phys.* **1987**, *86*, 6258.

(35) Johnson, B. R.; Winter, N. W. *J. Chem. Phys.* **1977**, *66*, 4116. Schatz, G. C. *J. Chem. Phys.* **1983**, *83*, 5677.

shown as the light dashed bell-shaped curves in Figure 1b. Their sum is the heavy dashed line, which to plotting accuracy is indistinguishable from the accurate quantal $\rho^0(E)$.

The value of κ_τ is shown above each feature in the fit in Figure 1b. Since nearly all of the values are close to one, we conclude that the quantized energy levels of the transition state are nearly ideal dynamical bottlenecks to the flow of reactive flux. (The value exceeds one for the last feature because higher-energy states are neglected in the fit.) Furthermore, all the flux, up to the highest energy, is associated with the peaks; i.e., there is no discernible background. In other words, the quantized transition state globally controls the reactive flux. Thus, exact quantum dynamics calculations provide validation for approximate theories[1-3,15-30] that postulate that quantized transition states control the dynamics of reaction.

Nature of the Transition States. A quantized transition state of H_3 is a short-lived species with a set of linear-triatomic quantum numbers[36] $[v_1v_2^K]$, which correspond to stretching (v_1), bending (v_2), and vibrational angular momentum (K). This labeling corresponds to the classical picture in which one degree of freedom, that corresponding to unbound motion along the reaction coordinate, is "missing" because a classical transition state is a hypersurface in phase space. [The implicit comparison is to a stable molecule like CO_2, which has quantum numbers $(v_1v_2^Kv_3)$,[36] with v_3 specifying the asymmetric stretch. The "missing" quantum number of the transition state reappears when we treat it more fully quantum mechanically as a resonance—see below.] Using a variety of methods, we were able to assign quantum numbers to the energy levels of the H_3 transition state with $J = 0$ and 1 up to 1.6 eV and with $J = 4$ up to 1.2 eV.[5,6]

The lowest-energy feature in $\rho^0(E)$ is the overall reaction threshold and is readily assigned as $[00^0]$. As a first step toward making the rest of the assignments, we correlated many of the features with thresholds in semiclassically computed vibrationally adiabatic potential energy curves.[7,15,18,19,22,23,28,37-42] The curves are defined by

$$V_a(v_1,v_2,J,s) = V_{MEP}(s) + \epsilon_{int}(v_1,v_2,J,s) \qquad (13)$$

where V_{MEP} is the Born–Oppenheimer potential energy along the reaction path and ϵ_{int} is the vibrational–rotational energy of the stretch, bend, and rotational modes excluding motion along the reaction coordinate. The reaction path is calculated by joining the steepest-descent paths in both directions from the saddle point in mass-scaled coordinates.[41] The stretching motion (with quantum number v_1) of the H_3 transition state correlates adiabatically with the vibrational motion (with quantum number v) in the reactant H_2 molecule.[39]

Five vibrationally adiabatic potential curves are shown in Figure 2, together with the quantized transition state spectrum $\rho^0(E)$

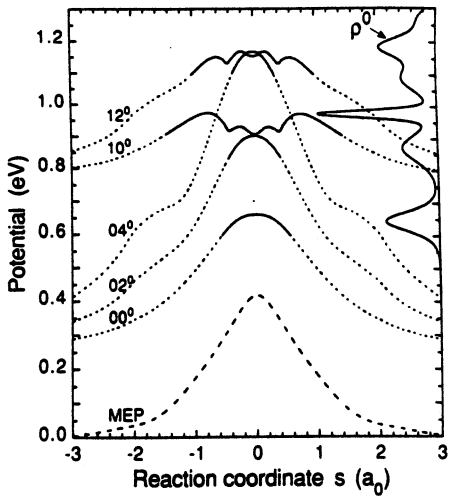

Figure 2. Vibrationally adiabatic potential curves for $H + H_2$, $J = 0$. The curves are shown as solid lines in the vicinity of potential maxima where the accurate collision dynamics is predominantly adiabatic and as dotted lines elsewhere. $V_{MEP}(s)$ is shown as a dashed curve. The density of reactive states is plotted vertically on the right to emphasize the correlation with vibrationally adiabatic thresholds.

oriented vertically so that the energy axes coincide. The thresholds (maxima in the potential curves) define vibrationally adiabatic transition state levels. It can be seen that the energies of the most prominent features in $\rho^0(E)$ coincide very closely with these levels. Thus, the reactive flux appears to be channeled in the interaction region through dynamical bottlenecks that are locally vibrationally adiabatic. However, since the quantal reaction is not globally adiabatic, the flux passing through a particular vibrational state of the transition state may originate from a wide set of reactant states. To emphasize this, we have shown the vibrationally adiabatic curves as dashed lines over much of the reaction coordinate s and as solid lines only near maxima in the potential curves. One way to understand why the dynamics is locally adiabatic in the vicinity of a barrier maximum is to note that at a threshold the reaction coordinate motion is classically stopped. Thus, the simplest criterion for vibrational adiabaticity, namely, that vibrational motions transverse to the reaction coordinate are fast compared to motion along the reaction coordinate, is locally satisfied.

The good agreement of the quantized transition state spectrum obtained from exact dynamics calculations with the maxima of vibrationally adiabatic potential curves even at high energies[5] has interesting implications about the usefulness of adiabatic approximations in general at high energies. In addition, it points to the way we might visualize quantized transition states. Vibrationally adiabatic justifications of transition state theory played an important role in its early history,[37,43] and Marcus showed that this kind of adiabaticity was capable of predicting the overall reaction threshold for collinear $H + H_2$ in both quantum mechanical[44] and classical[45] worlds. Later work, though, showed that global vibrational adiabaticity is not a good approximation at energies above the $v = 1$ product threshold.[46] When rotation and bends are present, we expect global adiabaticity to be even worse,[39,47] and it is,[17] but Schatz and Kuppermann showed that even in the 3D quantum world the adiabatic barrier height including bending zero-point energy is still a good predictor of the overall reaction threshold.[17] Garrett and one of the authors proved that reaction rates calculated by microcanonical variational theory, which makes no adiabaticity assumption, are the same as those obtained by assuming global vibrational adiabaticity,[18,48] so the

(36) The notation is standard [Herzberg, G. *Molecular Spectra and Molecular Structure. II. Infrared and Raman Spectra of Polyatomic Molecules*; D. van Nostrand: Princeton, 1945] except we use K instead of l because l is reserved for orbital angular momentum in collision theory. This quantum number is sometimes also called Ω.

(37) Eliason, M. A.; Hirschfelder, J. O. *J. Chem. Phys.* **1959**, *30*, 1426.
(38) Hofacker, L. *Z. Naturforsch. A* **1963**, *18*, 607.
(39) Marcus, R. A. *J. Chem. Phys.* **1965**, *43*, 1598. Marcus, R. A. *Discuss. Faraday Soc.* **1967**, *44*, 7.
(40) (a) Child, M. S. *Discuss. Faraday Soc.* **1967**, *44*, 68. (b) Garrett, B. C.; Truhlar, D. G.; Grev, R. S.; Magnuson, A. W. *J. Phys. Chem.* **1980**, *84*, 1730. (c) Smith, I. W. M. *Acc. Chem. Res.* **1990**, *23*, 101.
(41) Truhlar, D. G.; Kuppermann, A. *J. Am. Chem. Soc.* **1971**, *93*, 1840.
(42) (a) Truhlar, D. G.; Isaacson, A. D. *J. Chem. Phys.* **1982**, *77*, 3516. (b) Pollak, E.; Wyatt, R. E. *J. Chem. Phys.* **1983**, *78*, 4464. (c) Garrett, B. C.; Truhlar, D. G. *J. Chem. Phys.* **1984**, *81*, 309. (d) Steckler, R.; Truhlar, D. G.; Garrett, B. C.; Blais, N. C.; Walker, R. B. *J. Chem. Phys.* **1984**, *81*, 5700. (e) Garrett, B. C.; Truhlar, D. G. *J. Phys. Chem.* **1985**, *89*, 2204. (f) Garrett, B. C.; Truhlar, D. G. *Int. J. Quantum Chem.* **1986**, *29*, 1463. (g) Steckler, R.; Truhlar, D. G.; Garrett, B. C. *J. Chem. Phys.* **1986**, *84*, 6712. (h) Garrett, B. C.; Truhlar, D. G.; Varandas, A. J. C.; Blais, N. C. *Int. J. Chem. Kinet.* **1986**, *18*, 1065. (i) Garrett, B. C.; Truhlar, D. G.; Bowman, J. M.; Wagner, A. F. *J. Phys. Chem.* **1986**, *90*, 4305. (j) Haug, K.; Schwenke, D. W.; Shima, Y.; Truhlar, D. G.; Zhang, J.; Kouri, D. J. *J. Phys. Chem.* **1986**, *90*, 6757. (k) Truhlar, D. G.; Schwenke, D. W.; Kouri, D. J. *J. Phys. Chem.* **1990**, *94*, 7346.
(43) Hirschfelder, J. O.; Wigner, E. P. *J. Chem. Phys.* **1939**, *7*, 616.
(44) Marcus, R. A. *J. Chem. Phys.* **1964**, *41*, 610.
(45) Marcus, R. A. *J. Chem. Phys.* **1965**, *43*, 1598.
(46) Truhlar, D. G.; Kuppermann, A. *J. Chem. Phys.* **1970**, *52*, 3841.
(47) Wu, S.; Marcus, R. A. *J. Chem. Phys.* **1972**, *56*, 3519.
(48) Garrett, B. C.; Truhlar, D. G. *J. Phys. Chem.* **1979**, *83*, 1052.

lack of vibrational adiabaticity does not imply a breakdown of transition state theory for rate constants, for either microcanonical or canonical ensembles. Now, however, we find that even at high energy the microcanonical rate constants do show structure that correlates well with vibrationally adiabatic barrier maxima.[5] We conclude that the quantized transition states are well approximated by locally vibrationally adiabatic dynamical bottlenecks.

The role of excited-state vibrationally adiabatic barriers in determining thresholds for reactions of vibrationally excited diatomics has been well demonstrated,[42,49] and it has been shown that these adiabatic barrier maxima correspond to quantized quasiperiodic trajectories.[50] (In collinear reactions, these are actually periodic[51] and are called periodic orbit dividing surfaces.) The use of semiclassical correspondences should prove to be a powerful tool to understand vibrationally excited quantized transition states and dynamical bottlenecks in phase space[52] in general, and further work on this subject would be worthwhile.

It is well known that passage over a barrier is associated with a time delay in both classical and quantum mechanics, due to the slowing down of the system as it crosses the barrier top.[53] This time delay is manifest as an increasing phase (relative to the background phase) in selected elements of the scattering matrix or the eigenphases at the threshold for a chemical reaction.[54-57] Recently, it has been shown that time delays corresponding to passage over a barrier are associated with poles of the scattering matrix at complex energy.[58,59] The scattering matrix element S_{ji} is the coefficient of the outgoing wave in channel j for unit incoming wave in channel i. Thus, at a pole of the scattering matrix, the wave function is a pure outgoing wave in all channels. For this reason poles of the scattering matrix represent quantum mechanical resonances,[60-62] which may also be called metastable states or decaying states. In other words, quantized transition states are reactive scattering resonances.

We expect that the resonance picture of transition states, which is so new it has not been widely applied yet, will be a useful analytical tool and will provide new insights and computational approaches to the fundamental problems of reactivity. We note, however, that in many cases these resonances will not be isolated, narrow resonances, and that complicates[63] the analysis. In fact, the resonance picture is most useful when observable structure may be correlated with one or a small number of poles, i.e., when the resonance structure is resolvable. Our work shows that in many cases the transition state thresholds are resolvable. But analyses of the S matrix poles for passage over a barrier show that there is more than one pole associated with even a simple barrier.[58,59,64] One can associate the new quantum number v that labels the members of the sequence for a given parabolic or approximately parabolic barrier with the "missing" degree of freedom of the transition state. We then may ask whether the closest pole to the real axis is useful for explaining qualitative features of the observables. The study in ref 59 shows that it is. In addition, we may provide further evidence for this by using the parabolic model for quantized transition states in the H + H_2 reaction, as discussed in the next paragraph.

TABLE I: Transition State Lifetimes (fs) for H + H_2

J	E_r, eV	transition state resonance theory[a]	accurate[b]
0	0.65	10	11
	0.87	7	10
	0.98	28	28*
	1.09	6	5
	1.19	10	8
1	0.65	10	11
	0.76	8	9
	0.88	7	10
	0.98	27	28*
	0.99	6	8
	1.09	16	29*
	1.10	10	5
	1.19	10	8
	1.21	7	6

[a] From eq 17 and the W_r values of ref 6. [b] From ref 56. Notice that ref 56 used a slightly different potential energy surface than the one used in ref 6. For the three resonances marked with an asterisk the widths were determined in ref 69 by a resonance analysis of collisional delay times for the potential energy surface used in ref 6. Applying eq 15 to these widths yields Δt = 34, 32, and 6 fs, respectively, indicating that there is some uncertainty in this comparison due to the different potential surfaces and different measures of collision lifetime.

A complex resonance energy may be written as[61,62]

$$E = \mathcal{E} - (i/2)\Gamma \tag{14}$$

where $\mathcal{E}$ is the real part of the resonance energy and Γ is the resonance width, which is related to the collision lifetime Δt by[65]

$$\Delta t = 2\hbar/\Gamma \tag{15}$$

The scattering matrix poles for the potential of eq 6 are found at[58,64]

$$E_v = E_r - i\hbar|\omega_r|(v + \tfrac{1}{2}) \tag{16}$$

where v is the one-dimensional analogue of the "missing" quantum number v_3 mentioned above. Assuming that the v = 0 pole dominates the behavior of the reaction probability in this case and comparing (8), (14), (15), and (16) yields

$$\Delta t = 2/|\omega_r| = \hbar/(\pi W_r) \tag{17}$$

Using eq 17, we calculated Δt for several H + H_2 resonances from the W_r values of ref 6, which were obtained by fitting eqs 10 and 11 to accurate densities of reactive states defined by eq 12. These predicted lifetimes are listed in Table I, where they are labeled transition state resonance theory; they are compared there to Δt values calculated[56] from accurate quantum dynamical S matrix elements without using either transition state theory or resonance theory. The success of this calculation is by no means guaranteed, since the fits from which the W_r values are obtained require only

(49) (a) Garrett, B. C.; Truhlar, D. G. *J. Chem. Phys.* **1979**, *83*, 200. (b) Pollak, E. *J. Chem. Phys.* **1981**, *74*, 5586; (c) **1981**, *75*, 4435. (d) Skodje, R. T.; Schwenke, D. W.; Truhlar, D. G.; Garrett, B. C. *J. Phys. Chem.* **1984**, *88*, 628. (e) Skodje, R. T.; Schwenke, D. W.; Truhlar, D. G.; Garrett, B. C. *J. Chem. Phys.* **1984**, *80*, 3569. (f) Ashton, C. J.; Muckerman, J. T.; Schubert, F. E. *J. Chem. Phys.* **1984**, *81*, 5786. (g) Truhlar, D. G.; Brown, F. B.; Schwenke, D. W.; Steckler, R.; Garrett, B. C. In *Comparison of Ab Initio Quantum Chemistry with Experiment for Small Molecules*; Bartlett, R. J., Ed.; Reidel: Dordrecht, 1985; p 95. (h) Garrett, B. C.; Abusalbi, N.; Kouri, D. J.; Truhlar, D. G. *J. Chem. Phys.* **1985**, *83*, 2252.

(50) Pollak, E. *Chem. Phys. Lett.* **1982**, *91*, 27.

(51) (a) Pollak, E.; Pechukas, P. *J. Chem. Phys.* **1978**, *69*, 1218. (b) Pechukas, P. *Annu. Rev. Phys. Chem.* **1981**, *32*, 159.

(52) (a) Davis, M. J.; Gray, S. K. *J. Chem. Phys.* **1986**, *84*, 5389. (b) Davis, M. J. *J. Chem. Phys.* **1987**, *86*, 3978. (c) Skodje, R. T.; Davis, M. J. *J. Chem. Phys.* **1988**, *88*, 2429. (d) Gaspard, P.; Rice, S. A. *J. Chem. Phys.* **1989**, *90*, 2242. (e) Tersigni, S. H.; Gaspard, P.; Rice, S. A. *J. Chem. Phys.* **1990**, *92*, 1775. (f) Farantos, S. C.; Gomez Llorente, J. M.; Hahn, O.; Taylor, H. S. *J. Chem. Phys.* **1990**, *93*, 76. (g) Hahn, O.; Gomez Llorente, J. M.; Taylor, H. S. *J. Chem. Phys.* **1991**, *94*, 2608. (h) DeLeon, N.; Mehta, M. A.; Topper, R. Q. *J. Chem. Phys.* **1991**, *94*, 8310. (i) Davis, M. J.; Skodje, R. T. In *Intramolecular and Nonlinear Dynamics*; Hase, W. L., Ed.; JAI: Greenwich, 1991.

(53) Abusalbi, N.; Kouri, D. J.; Baer, M.; Pollak, E. *J. Chem. Phys.* **1985**, *82*, 4500.

(54) Levine, R. D.; Wu, S. *Chem. Phys. Lett.* **1971**, *11*, 557.

(55) Garrett, B. C.; Truhlar, D. G.; Grev, R. S.; Schatz, G. C.; Walker, R. B. *J. Phys. Chem.* **1981**, *85*, 3806.

(56) Cuccaro, S. A.; Hipes, P. G.; Kuppermann, A. *Chem. Phys. Lett.* **1989**, *157*, 440.

(57) Kuruoglu, Z. C.; Micha, D. A. *Int. J. Quantum Chem. Symp.* **1989**, *23*, 103.

(58) Atabek, O.; Lefebvre, R.; Garcia Sucre, M.; Gomez-Llorente, J.; Taylor, H. *Int. J. Quantum Chem.* **1971**, *40*, 211.

(59) Friedman, R. S.; Truhlar, D. G. *Chem. Phys. Lett.* **1991**, *183*, 539.

(60) Siegert, A. F. *Phys. Rev.* **1939**, *56*, 750.

(61) Newton, R. G. *Scattering Theory*; McGraw-Hill: New York, 1966.

(62) Taylor, J. R. *Scattering Theory*; John Wiley & Sons: New York, 1972.

(63) Feshbach, H. *Ann. Phys.* **1967**, *43*, 410.

(64) Seideman, T.; Miller, W. H. *J. Chem. Phys.* **1991**, *95*, 1768.

(65) Kuppermann, A. In *Potential Energy Surfaces and Dynamics Calculations*; Truhlar, D. G., Ed.; Plenum: New York, 1981; p 375.

reaction probabilities, without S matrix phase information, whereas the direct calculation of collisional delay times depends explicitly on phases. In addition, there is some ambiguity in such comparisons due to the precise definition of the collision lifetime[66] (and this is compounded in the present case by differences in the potential energy surface for the two calculations—see the footnote to Table I). Nevertheless, the general magnitudes and trends in the two columns of collision lifetimes are in reasonable agreement. This confirms the practical usefulness of resonance theory for treating transition states.

It is useful to distinguish the transition state resonance concept from the more traditional model[65] of a resonance, which involves a particle trapped behind a barrier or in a well. We may call the new class of resonances transition state resonances or thresholds. When we use the latter term, though, we must be careful to avoid confusion with the use of "threshold" to denote the opening of a specific state of reactants or products. In the transition state context, a threshold is rather the opening of a new level of the transition state. Denoting the two types of threshold as energetic threshold, when a new final state becomes energetically allowed, and dynamical threshold, when a reaction probability becomes significant for dynamical reasons more general than energetic accessibility of a final state, may be a useful way to distinguish them.

In our work on the H + H_2 reaction as well as our studies of one-dimensional scattering, we have found that the distinction between transition state resonances and trapped state resonances is not always unambiguous and a single resonance may partake of both characters. Nevertheless, the distinction is useful, just as the traditional subclassification[67] of trapped state resonances into single-particle and core-excited resonances has also stood the test of time. Transition state resonances tend to be broader than trapped state resonances, and for the chemical reactions considered explicitly in this paper both types of resonances are broad enough that the ideal resonance behavior embodied in the isolated narrow resonance (INR) formulas[61,62] is not expected to be observed.[68,69] Nevertheless, the more detailed characterization of transition states as broad resonances, e.g., by identifying their partial widths[61,62,70]—which in resonance theory control the decay probabilities into specific reactant and product states—is expected to be a fruitful area for future study.

Assignments and Interpretation of Peak Parameters. The correlation of the features in ρ^0 with the maxima of vibrationally adiabatic potential curves allows us to assign many of the low-bend states: [00^0], [02^0], [10^0], and [20^0] of the H_3 transition state (see Figures 1b and 2). Approximations in calculating the vibrationally adiabatic curves make the more highly bend-excited vibrationally adiabatic thresholds less accurate. It is possible, however, to assign the remaining energy levels using other methods.[5]

A completely assigned spectrum of the quantized transition state is shown for H + H_2, $J = 0$ in Figure 1b. We also show spectra for H + H_2, $J = 1$[6] in Figure 3a and for O + H_2, $J = 0$[9] in Figure 3b. The solid lines are the quantal results, and the dashed lines are fits. In all three cases the quantal and fitted curves are in excellent agreement. The O + H_2, $J = 0$ and H + H_2, $J = 0$ spectra are strikingly similar; the energy levels of the OH_2 transition state are somewhat more closely spaced since it contains a heavier atom. The $J = 0$ spectra include only even v_2 states, as for the $J = 0$ spectra of bound triatomics.[36] In the H + H_2, $J = 1$ spectrum, odd as well as even bend states appear. The energies of the even bend states agree very well with those for $J = 0$ when one takes into account that the larger value of the total angular momentum J shifts the energies of the states by an amount

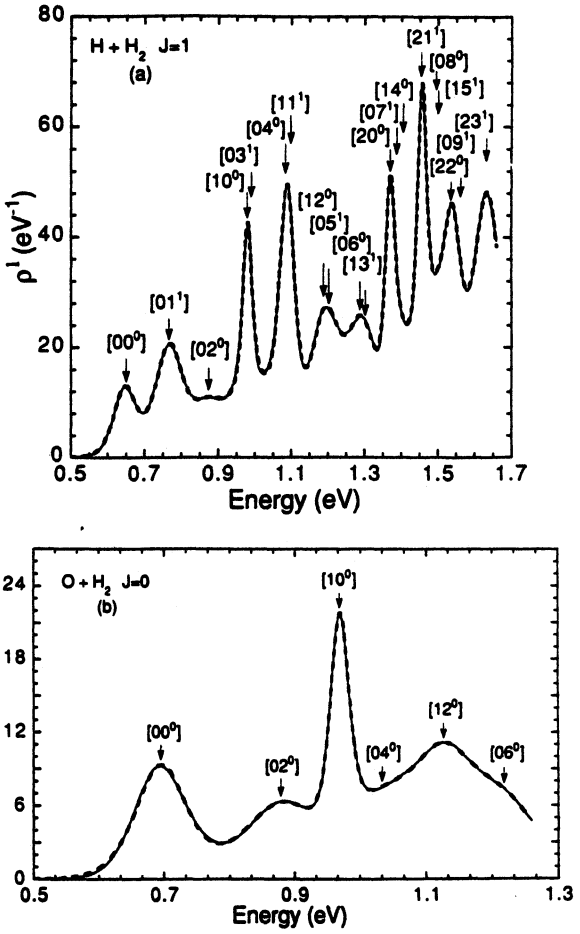

Figure 3. Density of reactive states and assignments for (a) H + H_2, $J = 1$ and (b) O + H_2, $J = 0$. The solid curves are spline fits to the accurate quantal results, and the dashed curves are the fits of (10) and (11). The positions of the fitted energy levels of the transition state [$v_1v_2^K$] are indicated by vertical arrows.

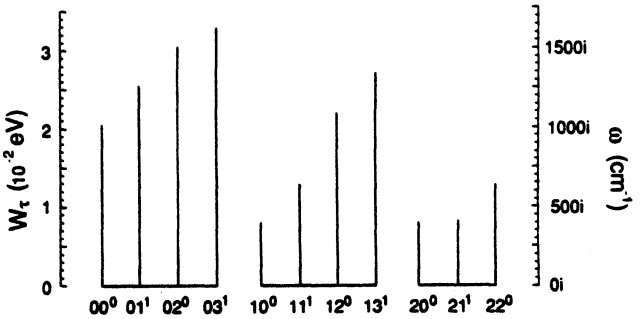

Figure 4. Values of the fitted width parameter W_r from (11) for H + H_2, $J = 1$, for the four lowest bend (v_2) levels in the stretch manifolds $v_1 = 0$ and 1 and for the three lowest bend levels in the stretch manifold $v_1 = 2$. The right axis gives the scale for interpreting these widths as imaginary frequencies of effective barriers.

$hcBJ(J + 1)$, where B is a rotational constant.[36]

Spectroscopic constants for the H_3 quantized transition state were obtained by fitting several of the assigned states to

$$E(v_1v_2)/hc = E_0/hc + \omega_1(v_1 + 0.5) + \omega_2(v_2 + 1) + x_{11}(v_1 + 0.5)^2 + x_{22}(v_2 + 1)^2 + x_{12}(v_1 + 0.5)(v_2 + 1) + BJ(J + 1) \quad (18)$$

where E_0 is a constant, and ω_1, ω_2, x_{11}, x_{12}, and x_{22} are the usual spectroscopic fit parameters.[36] The fit reproduces the energies within about 0.02 eV. We obtained $E_0 = 3061$, $\omega_1 = 2295$, $\omega_2 = 972$, and $B = 10.6$ (in cm^{-1}). These accurate quantal transition state parameters may be compared to the approximate values obtained by a conventional normal-mode analysis at the saddle point:[42h] $E_0 = 3372$, $\omega_1 = 2067$, $\omega_2 = 899$, and $B = 9.7$.

(66) Smith, F. T. *Phys. Rev.* **1960**, *118*, 349.
(67) Taylor, H. S.; Nazoroff, G. V.; Golebiewski, A. *J. Chem. Phys.* **1966**, *45*, 2872.
(68) Schwenke, D. W.; Truhlar, D. G. *J. Chem. Phys.* **1987**, *87*, 1095.
(69) Zhao, M.; Mladenovic, M.; Truhlar, D. G.; Schwenke, D. W.; Sharafeddin, O.; Sun, Y.; Kouri, D. J. *J. Chem. Phys.* **1989**, *91*, 5302.
(70) Garrett, B. C.; Schwenke, D. W.; Skodje, R. T.; Thirumalai, D.; Thompson, T. C.; Truhlar, D. G. *ACS Symp. Ser.* **1984**, *No. 263*, 375.

Equations 6, 8, and 9 show that the width parameter W_τ is inversely related to the effective barrier width. Figure 4 shows these parameters and is also labeled in terms of the imaginary frequencies ω_τ associated with the parabolic approximations to the barriers as computed by eq 8. This figure shows that the barrier width obtained in the fits tends to decrease as v_2 increases within a given stretch manifold v_1. This is consistent with the vibrationally adiabatic curves in Figure 2; as the bend quantum number increases, the curves become narrower. This is because the bending frequency is greatest at the saddle point geometry and decreases to zero at reactants and products, where the bending motion becomes a free rotation of the diatom. Since narrower barriers allow more tunneling, the bell-shaped curves $\rho_\tau(E)$ grow broader as bend excitation increases.

The final fit parameter is κ_τ, which also provides interesting information about dynamical bottlenecks. In fact, we found for H + H_2 that most of the breakdown of transition state theory is associated with only a few of the transition state levels, in particular the ones with highly excited bending motions. Being able to attribute the errors in transition state theory to specific levels of the transition state is an exciting new avenue of study.

In contrast to H + H_2 and O + H_2, the transition state spectra of the halogen–hydrogen halide[11-14] and He + H_2^+[10] reactions are much less resolvable, but the structure can be enhanced by viewing the density of reactive states under lower resolution.[10,11] This brings out the features due to the transition state dynamics occurring on the very short time scale that determines whether a system leaving the transition state region will eventually become a reactant or a product.

State-Selected Reactivity. It is possible to understand the reaction dynamics in greater detail by examining how flux through a given level of the transition state correlates with particular reactant and product states. We define a state-selected reaction probability, $P_n^J(E)$, for a given value of J by

$$P_n^J(E) = \sum_{n'} P_{nn'}^J(E) \tag{19}$$

and a state-selected density of reactive states $\rho_n^J(E)$ by

$$\rho_n^J(E) = \frac{d}{dE} P_n^J(E) \tag{20}$$

A typical state-selected density of reactive states is shown as the solid line in Figure 5, in this case for H + H_2, $J = 0$ and initial state ($v = 0, j = 4$), where j is the rotational quantum number. The prominent peaks in this spectrum coincide with transition state levels identified earlier, as indicated by the arrows. Thus, quantized levels of the transition state determine state-selected chemical reactivity as well as total reactivity. The figure indicates that reactive flux originating with (0,4) passes predominantly through only two levels ([02^0] and [20^0]) of the transition state at their threshold energies. In general, we find that a given reactant state couples primarily to only a few transition state thresholds.

To characterize quantitatively the coupling between reactant states and levels of the transition state, we fit the state-selected density with a functional form for scattering by effective potential energy barriers just as we did for the total density, eqs 10 and 11. The barrier height E_τ and width parameter W_τ were taken from the fit to the total density. The transmission coefficient parameter κ_τ was rewritten $\kappa_{\tau n}$ to indicate its association with reactant state n, and it was allowed to vary in the least-squares fit. The fitted value of $\kappa_{\tau n}$ is a measure of how much of the reactive flux at energy E_τ through transition state level τ originates in state n. A typical fitted state-selected density is shown as the dashed line in Figure 5. The fits reproduce the major peaks in the quantal densities reasonably accurately.

We have determined which reactant state–transition state couplings are most important for many transition state levels of H_3.[6] The most important diatomic states for the five lowest-energy transition state levels of H_3 are indicated in Figure 6. The thicker lines represent stronger couplings. When (v,j) states couple primarily to thresholds [$v_1v_2^K$] with $v = v_1$, we denote this as

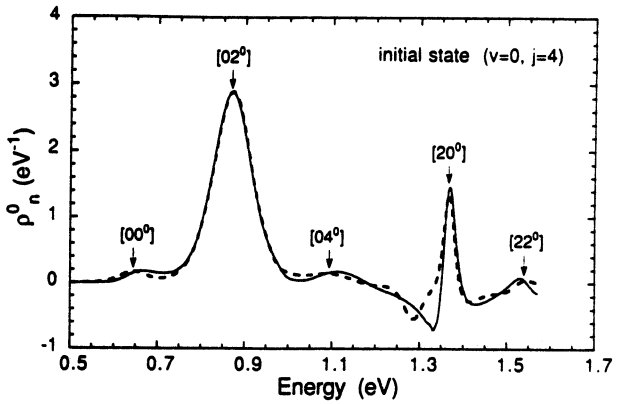

Figure 5. State-selected density of reactive states for H + H_2, $J = 0$ and initial state ($v = 0, j = 4$). The solid curve is a spline fit to accurate quantal results, and the dashed curve is the semiclassical fit. Features due to the dominant energy levels of the transition state [$v_1v_2^K$] are indicated.

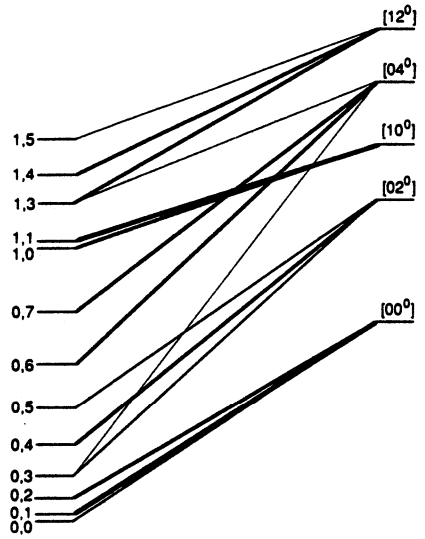

Figure 6. Channels making significant contributions to the total reactive flux passing through the five lowest-energy levels of the transition state for H + H_2, $J = 0$. Channels are labeled v,j and transition state energy levels [$v_1v_2^K$]. Thicker lines represent stronger couplings.

half-collision stretch adiabaticity. We find that for most energy levels of the transition state, only two or three initial states are primarily responsible for the reactive flux, and that stretch-adiabatic ($v = v_1$) couplings predominate. Stretch nonadiabaticity only begins to be significant for high v_1 within a given bend (v_2) manifold and for high v_2 within a given stretch (v_1) manifold. Only one of the couplings shown in Figure 6 is stretch-nonadiabatic, that between initial state (1,3) and transition state level [04^0]. The propensity for stretch adiabaticity in half-collisions[6] helps to explain previous work in which stretch-excited vibrationally adiabatic barrier maxima have been used successfully to predict reaction rates of vibrationally excited diatomics in several reactions.[18,42] The present work[5,6,9,11] places these vibrationally adiabatic dynamical bottlenecks in a more general perspective as special cases of quantized transition states. Examples are the third and seventh features in Figure 1b and the third feature in Figure 3b.

Initial state–transition state couplings are further characterized by a correlation between the reactants' rotational quantum number and the transition-state bend quantum number. For the H + H_2 reaction we have found that values of $|j - v_2| \leq 3$ are strongly favored for stretch-adiabatic half-collisions. This trend can be observed in Figures 5 and 6. In Figure 5, for instance, the dynamical reaction threshold for initial state (0,4) correlates with the [02^0] threshold ($|j - v_2| = 2$). Even though state (0,4) has a significant amount of relative translational energy, 0.231 eV, at the [00^0] threshold, coupling to this threshold is inhibited by

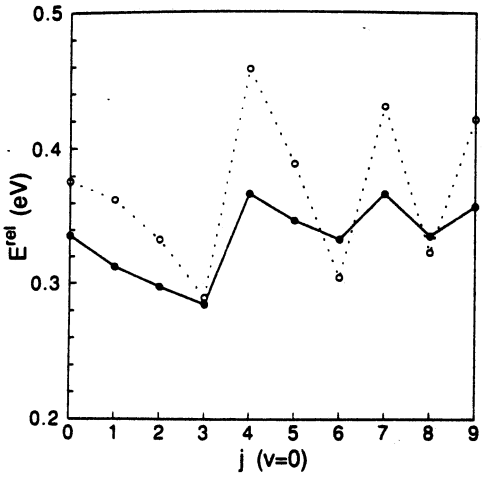

Figure 7. Relative translational energy at the dynamical reaction threshold for initial states ($v = 0, j = 0$–9) for H + H_2, $J = 0$. The solid curve is for the accurate quantum dynamical thresholds, which are defined as the energy at which the state-selected reaction probability first reaches 0.03. The dashed curve is for the transition state theory dynamical thresholds, which are defined as the lowest-energy level τ of the transition state for which $\kappa_{\tau n}$ is 0.03 or greater.

the large difference between j and v_2 ($|j - v_2| = 4$).

The latter observation can be used to show how quantized transition states allow one to understand important aspects of state-selected reactivity. For example, the solid curve in Figure 7 shows the relative translational energies for which the reaction probabilities $P_n^J(E)$ first reach a value of 0.03 for reactant rotational states $j = 0$–9 of the $v = 0$ vibrational level of H + H_2, $J = 0$. These translational thresholds are the major factor in determining the rate coefficients for these states, and so it is important to understand their trends. Why do they oscillate? Why is the first oscillation at $j = 4$? Consider the first transition state level τ to which a given initial state n has appreciable coupling. The dashed curve shows the relative translational energy at the lowest level of the transition state for which the transmission coefficient $\kappa_{\tau n}$ is 0.03 or greater. The solid and dashed curves exhibit maxima and minima at the same values of j. Thus, we see that the dynamical couplings of individual reactant states to specific levels of the transition state explain the trends in the dynamical thresholds for state-selected reactivity. For example, the relative translational energy decreases as j is incremented from 0 to 3 because the flux out of these initial states is focused through the [00^0] threshold. When j is incremented to 4, though, the relative translational energy at the dynamical threshold increases because the flux is focused through the [02^0] threshold, which lies 0.227 eV above the [00^0] threshold. Figure 7 demonstrates that state-selected reactivity is correlated with transition state energy levels up to high j. The insights offered by quantized transition state analysis into the dependence of rate constants on initial rotational quantum number are particularly welcome since this subject is not nearly as well understood as the effect of vibrational excitation on reactivity.

Summary

Quantized transition state features have been identified in the accurate quantum dynamics for several reactions based on accurate quantum dynamics calculations of the microcanonical rate constants. The new approach that reveals these states most clearly is the calculation of the density of reactive states. We have found that, individually, the quantized levels of the transition state gate the reactive flux with near unit efficiency and that, together, they globally control chemical reactivity for the entire range of energies relevant to thermal rate constants up to high temperature. This interpretation of exact quantum mechanical results provides a foundation for approximate theories such as variational transition state theory which are based on the postulate that quantized transition states control chemical reactivity. In addition, the propensities for selected reactant states to react via particular levels of the transition state provide a more detailed understanding of state-selected reactivity trends.

Acknowledgment. We are grateful to Bruce C. Garrett and Gillian C. Lynch for collaboration on some parts of this work. This work was supported in part by the National Science Foundation, NASA, the Minnesota Supercomputer Institute, and the Army High Performance Computing Research Center.